AGU PUBLICATIONS

Global Biogeochemical Cycles

RESEARCH ARTICLE
10.1002/2016GB005445

Key Points:
- Visibility data can be used as proxy for annual fire emissions in the Amazon
- Fire emissions here were low up to the late 1980s and increased afterwards with substantial interannual variability
- Fire-driven deforestation in the 1970s and 1980s was lower than found in other data sets

Correspondence to:
M. J. E. van Marle,
m.j.e.van.marle@vu.nl

Citation:
van Marle, M. J. E., R. D. Field, G. R. van der Werf, I. A. Estrada de Wagt, R. A. Houghton, L. V. Rizzo, P. Artaxo, and K. Tsigaridis (2017), Fire and deforestation dynamics in Amazonia (1973–2014), *Global Biogeochem. Cycles*, *31*, 24–38, doi:10.1002/2016GB005445.

Received 6 MAY 2016
Accepted 12 NOV 2016
Accepted article online 16 NOV 2016
Published online 12 JAN 2017

Fire and deforestation dynamics in Amazonia (1973–2014)

Margreet J. E. van Marle[1], Robert D. Field[2,3], Guido R. van der Werf[1], Ivan A. Estrada de Wagt[1], Richard A. Houghton[4], Luciana V. Rizzo[5], Paulo Artaxo[6], and Kostas Tsigaridis[3,7]

[1]Faculty of Earth and Life Sciences, Vrije Universiteit Amsterdam, Amsterdam, Netherlands, [2]Department of Applied Physics and Applied Mathematics, Columbia University, New York, New York, USA, [3]NASA Goddard Institute for Space Studies, New York, New York, USA, [4]Woods Hole Research Center, Falmouth, Massachusetts, USA, [5]Department of Exact and Earth Sciences, Universidade Federal de Sao Paulo, Sao Paulo, Brazil, [6]Physics Institute, Universidade de Sao Paulo, Sao Paulo, Brazil, [7]Center for Climate Systems Research, Columbia University, New York, New York, USA

Abstract Consistent long-term estimates of fire emissions are important to understand the changing role of fire in the global carbon cycle and to assess the relative importance of humans and climate in shaping fire regimes. However, there is limited information on fire emissions from before the satellite era. We show that in the Amazon region, including the Arc of Deforestation and Bolivia, visibility observations derived from weather stations could explain 61% of the variability in satellite-based estimates of bottom-up fire emissions since 1997 and 42% of the variability in satellite-based estimates of total column carbon monoxide concentrations since 2001. This enabled us to reconstruct the fire history of this region since 1973 when visibility information became available. Our estimates indicate that until 1987 relatively few fires occurred in this region and that fire emissions increased rapidly over the 1990s. We found that this pattern agreed reasonably well with forest loss data sets, indicating that although natural fires may occur here, deforestation and degradation were the main cause of fires. Compared to fire emissions estimates based on Food and Agricultural Organization's Global Forest and Resources Assessment data, our estimates were substantially lower up to the 1990s, after which they were more in line. These visibility-based fire emissions data set can help constrain dynamic global vegetation models and atmospheric models with a better representation of the complex fire regime in this region.

1. Introduction

In their natural state, tropical rainforests rarely burn, because of moist conditions underneath the canopy and because dry lightning is rare [*Cochrane*, 2003]. Human settlements leading to, for example, agriculture and road development in general lead to increased ignitions [*Moran*, 1993]. One way is the slash-and-burning method where small-scale patches of forest are burned and used for several years for agricultural purposes. At a later stage, large-scale deforestation aided by fire occurred, where forest is removed permanently for industrial-scale crop production. Currently, fire-driven deforestation is the main source of carbon emissions in Amazonia [*Morton et al*., 2006, 2008; *Cochrane*, 2009; *van der Werf et al*., 2010]. It is often assumed that fire emissions have increased over time here, but the timing and pattern of this increase is not well known. Anthropogenic fire regimes in the rainforests make the ecosystem more vulnerable for fire [*Nepstad et al*., 1999] and may increase the occurrence of fire-prone conditions due to the effects of emitted aerosols on precipitation formation [*Bevan et al*., 2009; *Gonçalves et al*., 2015].

The Amazon region has been deforested by about 15% from 1976 to 2010 and deforestation is one of the drivers of changing energy and water cycles in the southern and eastern portions of the Amazon basin [*Davidson et al*., 2012; *Aragão et al*., 2014]. Satellite-based forest loss data sets show substantial interannual variability (IAV) over the 1990s and 2000s and an overall decrease after 2005 as a result of reduced deforestation rates in Brazil due to conservation policies, namely, stricter law enforcements and expansion of the governmental protection of the Amazon area [*Nepstad et al*., 2009; *Hansen et al*., 2013]. Although forest loss has decreased in Brazil, neighboring Argentina, Paraguay, and Bolivia show an increase over the 2000s [*Chen et al*., 2013; *van Marle et al*., 2016]. Nowadays, deforestation in the Amazon often goes hand in hand with fire, emitting particulate matter into the atmosphere, which reduces air quality and can affect human health [*Johnston et al*., 2012; *Marlier et al*., 2012]. *Reddington et al*. [2015] showed that the reduction in Brazilian fire emissions related to the decrease in deforestation fires prevented 400 to 1700 premature adult deaths annually.

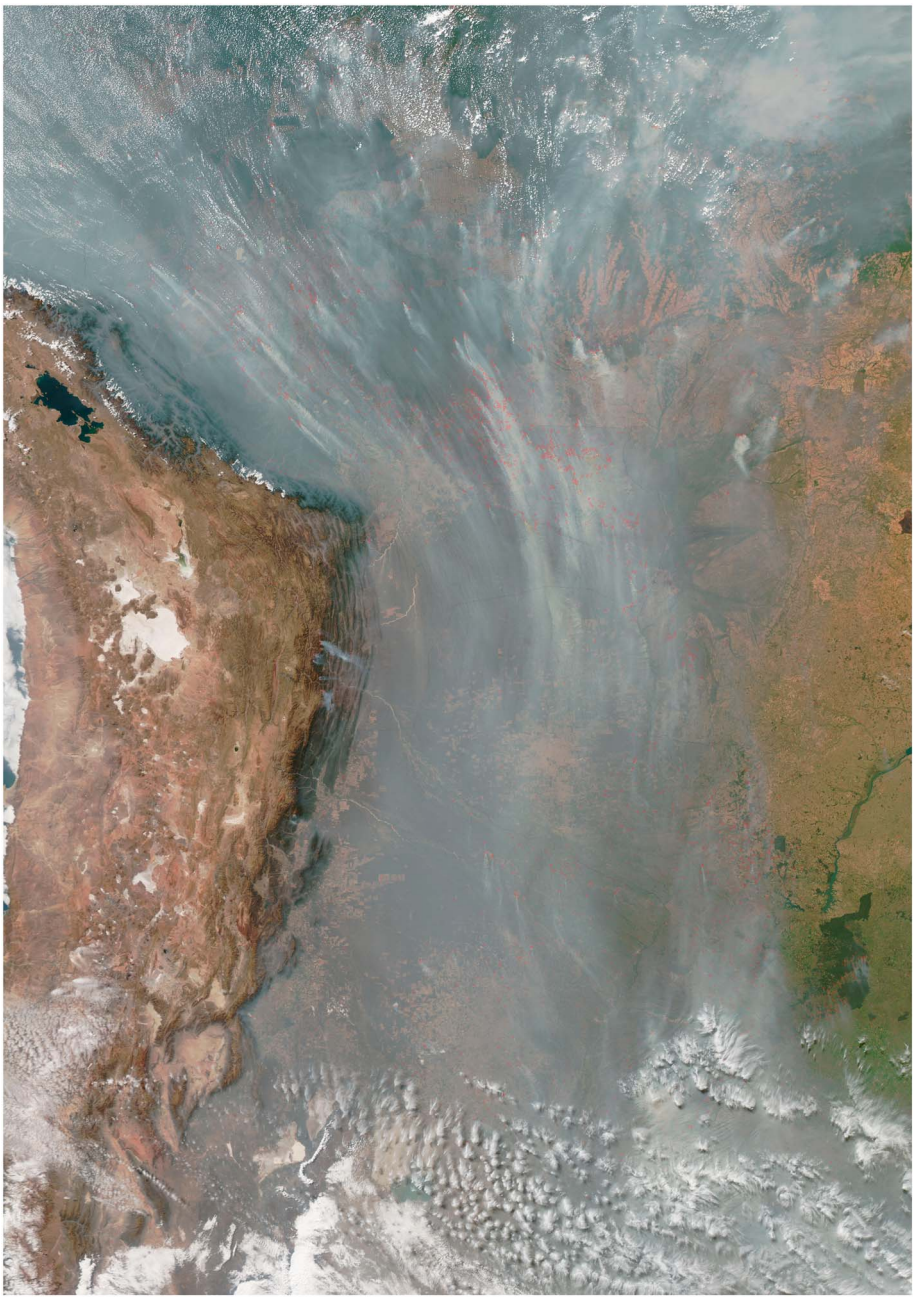

Figure 1. Smoke from fires in Bolivia and Brazil (states of Rondônia and Mato Grosso) observed by MODIS during the 2010 fire season. Highest concentrations are seen east of the Andes where smoke from fires farther north and east is funneled southward. The region covered by this image is outlined in Figure 2. NASA image courtesy: Jeff Schmaltz.

To understand how fires influence and interact with the Earth system and specifically the atmosphere, quantitative information on emissions and a breakdown of emissions into different sources is required. These can be derived using satellite-observed burned area or active fires potentially in combination with biogeochemical modeling, as done in, for example, the Global Fire Emissions Database (GFED) or the Global Fire Assimilation System [*van der Werf et al*., 2010; *Kaiser et al*., 2012]. Alternatively, atmospheric concentrations of trace gases and aerosols, partly influenced by fire emissions, can also be observed by satellites directly. The Measurements Of Pollution In The Troposphere (MOPITT) sensor is often used for this purpose and observes carbon monoxide (CO) from space. It has shown to be related to South American biomass burning

emissions [*Edwards et al*., 2006]. Other examples include the Microwave Limb Sounder that can observe variations in CO and ozone with increased CO emissions over the Amazon region for 2004, 2005, 2007, and 2010 [*Livesey et al*., 2013] and the aerosol index observed by the various sensors.

However, these data sets only provide data for the satellite era, which starts for the sensors or data sets mentioned above in 1997 or later. Information about fire emissions in the historic record before that time is mainly based on country-level statistics. A widely used metric is the deforestation and afforestation inventory of the Food and Agricultural Organization's (FAO) Global Forest and Resources Assessment (FRA) [*Food and Agriculture Organization of the United Nations*, 2012], where country-scale estimates of forest loss and gain area are converted to carbon emissions via a bookkeeping model [*Houghton*, 2003]. While several proxies exist that provide information before the satellite period (e.g., charcoal-based records from lake-sediment and levoglucosan from ice core records), for the Amazon region only charcoal [*Power et al*., 2010; *Marlon et al*., 2013] and historical [*Mouillot and Field*, 2005] records have been constructed. The latter suggests that burned area or fire in general has increased slowly over the 1960s and 1970s and increased more strongly over the 1980s and 1990s. This data set lacks information about interannual variability (IAV), which limits our ability to understand the contributions of different possible drivers of fire activity, for example, land use and climatic factors.

In this study we used horizontal visibility data observed by the World Meteorological Organization (WMO) weather stations throughout the Amazon region to reconstruct a fire history for this region since 1973. Horizontal visibility are human observations using landmarks with known distances during the day and using point light sources at night [*World Meteorological Organization*, 1996]. Horizontal visibility is influenced by several sources including dust, air pollution, haze, fog, and precipitation. Fires also have a strong impact on visibility as shown in Figure 1: an image of Bolivian fires taken from the Moderate Resolution Imaging Spectroradiometer (MODIS) during the 2010 fire season. Visibility data sets are inherently more subjective than more conventional weather station records but have shown to be useful in a wide range of studies constraining regional air quality changes [*Doyle and Dorling*, 2002; *Che et al*., 2007; *Chang et al*., 2009], desert dust emissions [*Mahowald et al*., 2007], and global trends in atmospheric haze [*Li et al*., 2016].

Our goal was to determine the extent to which visibility observations could be used to constrain fire emissions in the main deforestation region of the Amazon. This has shown to be the case for peat fires in Indonesia [*Heil and Goldammer*, 2001; *Field et al*., 2009, 2016]. The fire regime in Indonesia is strongly linked to anthropogenic use of fire for deforestation and peatland cultivation and rainfall patterns. New estimates of fire emissions and their temporal pattern in Amazonia may help to understand longer-term fire dynamics, which we do here in the context of estimates of deforestation. We also anticipate that the record can be used to evaluate models that require information about fire and deforestation dynamics in this region, including biogeochemical, atmospheric, and Earth system models, especially those with prognostic fire models.

2. Methods

2.1. Horizontal Visibility Observations

We obtained raw, synoptic weather station records from the NOAA National Climatic Data Center Integrated Surface Database (https://catalog.data.gov/dataset/integrated-surface-global-hourly-data), which is composed of data from WMO-level surface stations provided by national meteorological agencies. While 55 WMO stations in our study region [7°S–17°S, 48°W–68°W] were available, many were excluded after applying our selection criteria as described below. Out of 55 stations 18 were found suitable and are depicted in Figure 2 and cover the areas with the highest total particulate matter (TPM) emissions based on the annually averaged Global Fire Emissions Database version 4 with small fires (GFED4s) over 1997–2014 (updated version of *van der Werf et al*. [2010]). Data filtering and station selection was based on three steps.

1. The individual observations were filtered and adjusted as in *Husar et al*. [2000] where observations that contained flags for rain or wet fog (relative humidity (RH) $>$ 75%) were excluded, as were observations with RH $>$ 90% or precipitation $>$ 2.5 mm over the day. Furthermore, records with missing dew point or

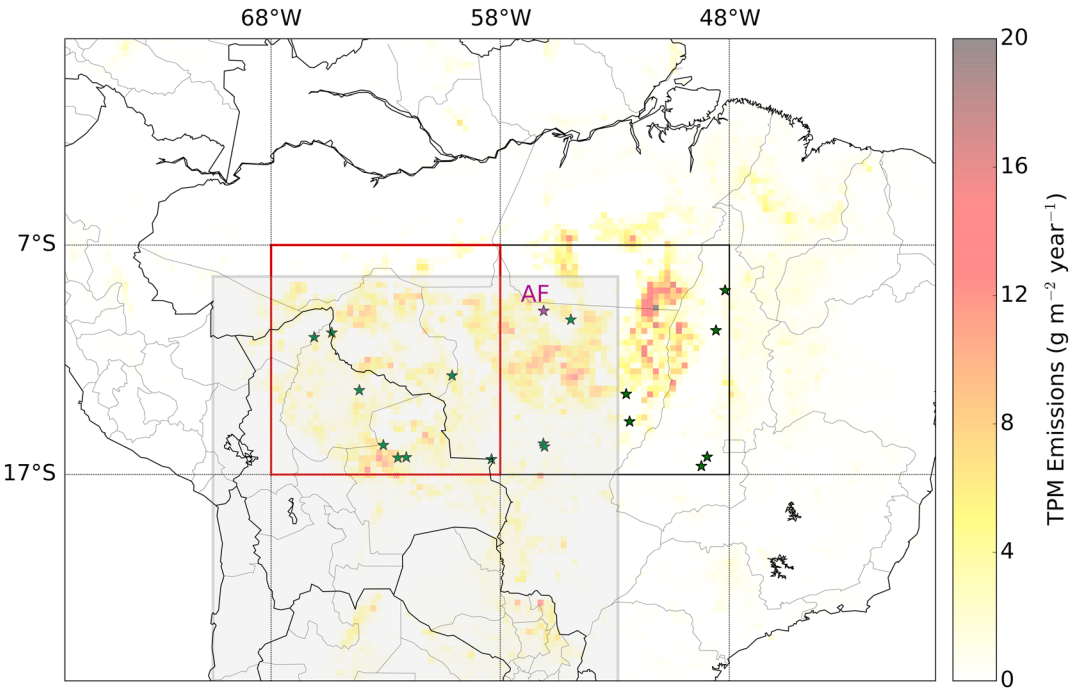

Figure 2. Locations of WMO stations used in our analysis indicated by the stars. The purple star denotes Alta Floresta (AF), for which surface particulate matter measurements were available (Figure 4). The color shading shows the average annual GFED4s TPM emissions per 0.25° × 0.25° grid cell over 1997–2014. The gray box shows the region covered by Figure 1.

air temperature data were removed, because these are needed to calculate RH. Visibility records of 0 m were replaced by a set minimum of 50 m, the next lowest reported value, necessary for calculating extinction coefficients (described below), and we used a uniform maximum value of 20 km. Finally, to exclude years with missing landmarks or not enough observations to account for seasonality, we removed years with a variance less than 5 km.

2. Observations are often done at irregular time intervals, which vary per day, year, and station. For consistency we therefore aggregated the individual observations to one daily average.
3. The average daily observations were subsequently manually inspected for temporal inconsistencies and sudden jumps in the signal, which could be the result of, for example, a change in landmarks being used to estimate visibility. Horizontal visibility can be influenced not only by fire but also by various other sources, such as dust and fog, and is influenced by the observers' interpretation. This subjectivity introduces a random component in the signal. Also, when observations were too fragmented (for example, some stations were lacking observations during the fire season or only had continuous observations shorter than 1 year with gaps of several years) or when the maximum distance recorded was smaller than 12 km, stations were excluded [*Husar et al.*, 2000].

To focus on low-visibility events and to correct for limitations of the human eye and imperfections of the landmarks, the observations in meters were then converted to the more often used extinction coefficient (B_{ext}) in km^{-1} using the Koschmeider relationship (equation (1)), where HV is the horizontal visibility in km and the Koshmeider constant (K) was set to a value of 1.9 [*Husar et al.*, 2000; *Schichtel et al.*, 2001].

$$B_{ext} = \frac{K}{HV} \quad (1)$$

We constructed our monthly record from 1973 to 2014, the period over which most stations had data albeit with gaps of various lengths of time (Figure 3). We took the median B_{ext} over the selected stations in the region [7°S–17°S, 48°W–68°W], the region with the highest fire emissions over 1997–2014 according to GFED4s. We also split this region into eastern and western halves to identify possible differences in fire activity and relationships to satellite data within the larger Amazon region.

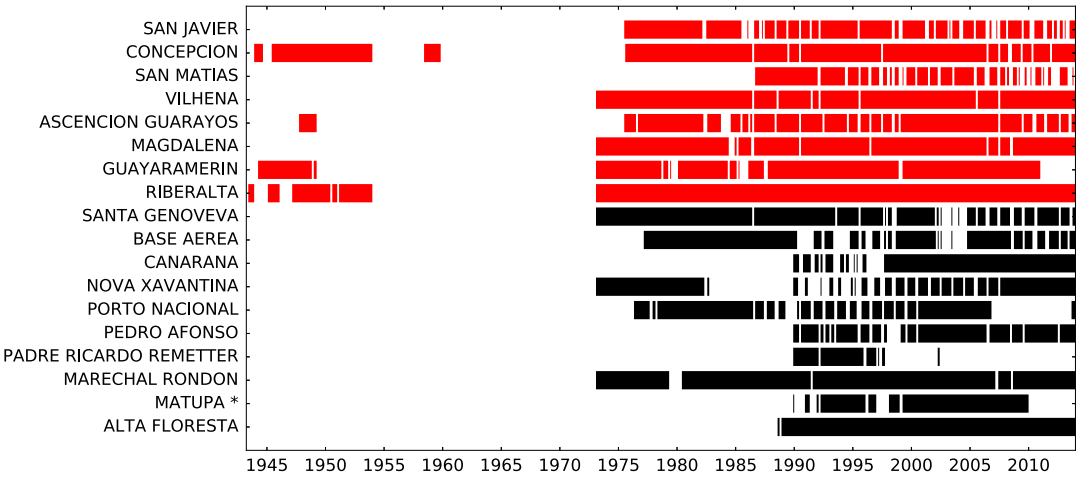

Figure 3. Temporal coverage of the selected WMO stations before filtering the data. The stations located in the western box of Figure 2 are in red, those in the eastern box in black.

2.2. Relationships Between Visibility and Satellite-Observed Data

Total particulate matter (TPM) emissions were derived from the Global Fire Emissions Database version 4s (GFED4s). TPM is a measure for all particles smaller than 100 μm, and this data set comes closest to what the human eye can see and what is thus represented in the visibility data set. GFED is based on the Carnegie-Ames-Stanford-Approach (CASA) biogeochemical model and uses burned area derived from MODIS and other climate variables as input to compute dry matter (DM) carbon emissions [*van der Werf et al.*, 2010; *Randerson et al.*, 2012; *Giglio et al.*, 2013]. The DM emissions are then converted to TPM emissions via emission factors for different biomes within a grid cell [*Akagi et al.*, 2011]. GFED4s starts in 1997 with a monthly time step.

We compared the GFED TPM emissions with the aggregated B_{ext} for the whole study region (Figure 2) to understand how well they covaried and to get an indication of how B_{ext} relates to TPM emissions. The comparison of B_{ext} values with fire emissions was done for the dry season, thus the fire season, without taking atmospheric transport into account.

We also compared the visibility data set to total column CO observations retrieved from the MOPITT satellite as an independent constraint on fire emissions. CO is released from incomplete combustion of vegetation and fossil fuels, and fires substantially enhance the CO concentration over background conditions. CO observations from MOPITT have shown to be able to capture IAV in emissions in regions which are heavily impacted by biomass burning [*Edwards et al.*, 2006; *Logan et al.*, 2008; *Mieville et al.*, 2010; *Liu et al.*, 2011]. We used total column observations of CO for the months June–October from 2000 to 2014 in our comparison.

In situ surface measurements of particulate matter mass concentrations with an aerodynamic diameter smaller than 10 μm (PM_{10}) were also available for August 1992 to February 2005 in Alta Floresta (Brazil, State of Mato Grosso, 9.871°S, 56.104°W, 277 m above sea level), which provided a nonsatellite record for comparison, and extending further back than GFED or MOPITT [*Artaxo et al.*, 1994; *Maenhaut et al.*, 2002; *Martin et al.*, 2010]. The particles sampled in Teflon filters were analyzed by gravimetry with filter explosion times ranging from 1 to 10 days. Summed uncertainties were estimated to be 15% of PM_{10} mass concentrations, based on uncertainties in calibration of the mass flowmeters (5%) and elemental and mass analysis (10%, including filter handling).

In our approach, we assumed that potential changes in wind patterns are of second-order importance and have thus not been taken into account. This is supported by visual inspection of surface wind patterns derived from the National Centers for Environmental Prediction/National Center for Atmospheric Research (NCEP/NCAR) reanalysis [*Kalnay et al.*, 1996]. From June to October the general wind pattern was relatively constant over our study period, with light winds from the east bending southward when reaching the Andes. Future work, using an atmospheric transport model and observed wind patterns, could lower the uncertainty arising from not taking variability in atmospheric transport into account.

2.3. The Role of Deforestation as a Driver of Fire Emissions

To understand the role of deforestation as a driver of fires and potentially also to yield information on how deforestation may have changed over time, we compared the visibility-based emissions with two forest loss data sets over the Brazilian Amazon and one data set of carbon emissions related to deforestation. We only used data sets which cover a relatively long time period from at least the 1990s onward.

First, we compared our results to net forest loss based on passive-microwave satellite observations of vegetation optical depth (VOD), which has shown to be sensitive to changes in biomass density [*Liu et al*., 2015]. The VOD-based deforestation data set we used here [*van Marle et al*., 2016] provides annual estimates of net forest loss, which is the net result of deforestation, forest degradation, and regrowth within a grid cell, on a $0.25° \times 0.25°$ resolution for all of South America from 1990 to 2010. Interannual VOD changes over the region agreed reasonably with the Global Forest Change data set derived from Landsat, during the overlapping period since 2001 [*Hansen et al*., 2013]. VOD data for 1991 were missing, because the eruption of Mount Pinatubo influenced the passive microwave signal.

The second data set we compared our results with is the Program for Deforestation Assessment in the Brazilian Legal Amazon with Satellite Imagery (PRODES), which is developed by the Brazilian National Institute for Space Research (INPE). PRODES estimates annual deforestation events of primary forest larger than 6.25 ha based on a multidata approach utilizing Landsat data, supplemented by data from the China-Brazil Earth Resource Satellite and from the UK-DCM2 from the Disaster Monitoring Constellation International Imaging [*Shimabukuro et al*., 1998]. PRODES provides data from 1989 onward, although no data are available for 1992. In this study we used the summed total of the provinces of Acre, Mato Grosso, Rondônia, Pará, and Tocantins, the provinces within the Amazonia Legal closest to our study region (Figure 2), from 1989 to 2014. PRODES does not include Peru and Bolivia, which were part of our study region.

Finally, we compared our results, including decadal changes, with the updated country-scale carbon emission estimates associated with deforestation fires based on the bookkeeping method of *Houghton* [2003] using deforestation rates reported by the FRA 2015. For further details on the collection and validation of national data for FRA2015 see *MacDicken* [2015]. Deforestation is defined there as the conversion from forest to some other land cover. The rates are based on changes in forest area over a period of 5 years. In *Houghton* [2003] annual changes in cropland and pastures are used to provide year-to-year differences in deforestation rates. Deforestation is then assigned to forest types (i.e., biomass densities), and a fraction (35%) of that biomass is assumed to be burned [*Houghton et al*., 1991; *Houghton*, 2003]. The updated data set is not published yet. For comparisons with the western box and for the whole region we used the total of Bolivian and Brazilian country estimates. For the eastern box only the Brazilian estimates were used.

For the comparison on a decadal scale we converted the visibility-based results to carbon emissions by converting the B_{ext} to TPM emissions based on their linear relationship found per $10° \times 10°$ box and subsequently converting the TPM emissions to carbon emissions based on the emissions factors used within GFED (drawn largely from *Akagi et al*. [2011]). The converted visibility-based carbon emissions were then compared with the summed FAO-based carbon emissions for Bolivia and Brazil.

Forest loss is not occurring at the same location every year and spatial variability in deforestation and fire occurrence could thus impact the visibility signal. We calculated the mean weighted distance from pixels with VOD-based forest loss to the WMO stations which revealed that the average distance was relatively stable with 550 ± 43 km (1σ) between deforestation and observations for the western box and 614 ± 39 km (1σ) for the eastern box without a clear increasing or decreasing trend over time. We therefore assumed in this study that the effect of a changing deforestation front did not influence B_{ext} substantially, but we do acknowledge that this is a source of uncertainty, especially for the 1970s and 1980s.

4. Results

4.1. Visibility as Fire Indicator Over the South American Burning Region

Figure 4a shows the visibility-based B_{ext} and GFED TPM fire emissions for the whole region (Figure 2). These visibility-based results are averaged over the two boxes, because B_{ext} behaved slightly different for the two grid boxes, see section 4.2. Over this large region, the B_{ext} signal explained 47% of the variability in GFED TPM (Table 1). The background value of B_{ext} is around 0.1, which corresponds to an average visibility of 19 km

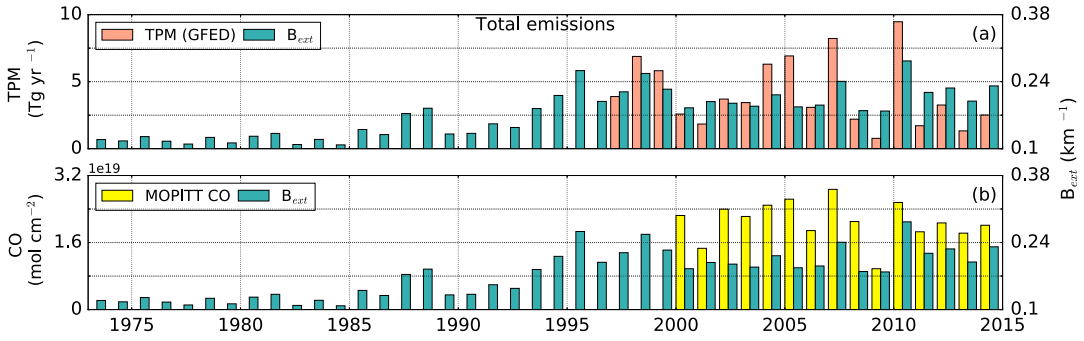

Figure 4. Averaged B_{ext} values for the whole study region [7°S–17°S, 48°W–68°W], compared with (a) GFED-based TPM emissions (1997–2014) and (b) MOPITT CO concentrations (2000–2014) for the same region.

(equation (1)), thus very close to the 20 km maximum value for visibility. Both GFED TPM and visibility-based B_{ext} capture the high-fire years 1998, 2004, and 2010. The biggest discrepancies are in 2001, where B_{ext} shows relatively high values and the fire years 2005 and 2007 where GFED is higher (Figure 4a). The B_{ext} signal explained less (18%) of the MOPITT CO over 2000–2014 (Figure 4b), although both data sets captured the peak in fire emissions in 2010 (Table 1). Years where MOPITT CO shows relatively high values are 2000, 2005, and 2007, and the visibility-based estimate is relatively high in 2001. The correlation improves when we take only the western region into account as will be explained later.

Before the fire satellite era, beginning in 1997, visibility-based estimates indicate that fire emissions were relatively low until 1987 and 1988. Those 2 years were the first relatively high-fire years in the B_{ext} record, followed by a few low-fire years after which fire emissions started to increase during the 1990s, with 1995 as peak year over the 1990s (Figure 4). After 1995 fire emissions remained elevated above the pre-1987 values, but with substantial IAV. During the 2000s there is, in general, a decreasing trend toward the end of the record although 2010 was the highest fire year in our data set.

4.2. Subregional Visibility-Fire Relationships

To illustrate how visibility relates to local aerosol load, Figure 5 shows the visibility from the Alta Floresta station marked with "AF" in Figure 2. Seasonality is evident in most years, with higher B_{ext} values during the dry fire season and lower values during the wet season. We compared the visibility signal from Alta Floresta with ground-based measurements of PM_{10} at the same station (15% uncertainty based on summed estimated uncertainties for sampling method and analysis), and the IAV is captured reasonably well with Pearson $r^2 = 0.84$ on a monthly time step (Figure 5) and $r^2 = 0.79$ for annual summed values.

Separating the analysis between western (Figure 6) and eastern (Figure 7) parts of the large burning regions, and for the dry season only, led to different correlations between B_{ext}, TPM and CO (Table 1). Both the western and eastern boxes had a higher agreement for the dry months only, June to October (Figures 6b and 7b), with $r^2 = 0.61$ for the western box and $r^2 = 0.40$ for the eastern box, compared to all monthly observations (Figures 6a and 7a). The 5 months during the dry season account for 98% and 95% of all GFED TPM emissions for the western and eastern boxes, respectively. For the dry season, monthly averaged B_{ext} values were converted to TPM emissions according to equations (2) and (3) for the western and eastern boxes, respectively. The negative intercept in the equations is due to nonfire impacts on visibility.

Table 1. Correlations Between Visibility-Based B_{ext} Observations and Monthly As Well As Annual Summed GFED TPM Emissions (1997–2014) for June–October and Monthly and Annual Summed MOPITT CO (2000–2014) for June–October

Visibility-Based r^2	West [7°S–17°S, 58°W–68°W]		East [7°S–17°S, 48°W–58°W]		Total Region [7°S–17°S, 48°W–68°W]
	Annual	Monthly	Annual	Monthly	Annual
GFED TPM	0.47* (*p*)	0.61* (*p*)	0.16 (*p*)	0.40* (*p*)	0.47* (*p*)
MOPITT CO	0.32* (*p*)	0.42* (*p*)	0.03 (*p*)	0.34* (*s*)	0.18 (*p*)

*Pearson (*p*) or Spearman (*s*) correlation significant at $p < 0.01$.

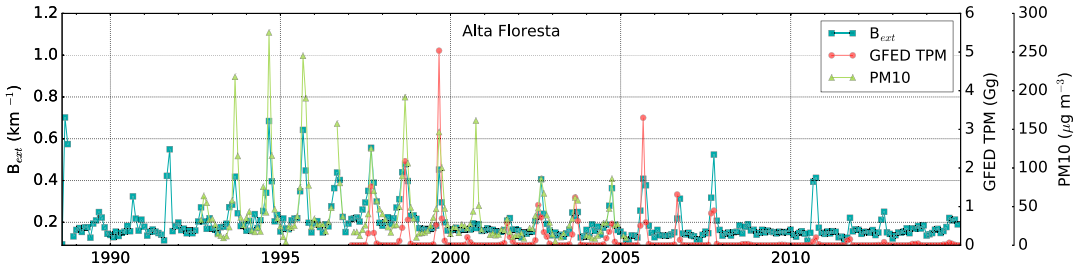

Figure 5. Monthly averaged B_{ext} and ground-based measurements of PM_{10}, both observed at Alta Floresta, and averaged GFED TPM emissions for the 36 0.25° × 0.25° grid cells centered over Alta Floresta.

$$\mathrm{TPM_{visibility}} = -8.2\mathrm{E11} + 5.36\mathrm{E12} * B_{\mathrm{ext}} \quad (2)$$

$$\mathrm{TPM_{visibility}} = -6.7\mathrm{E11} + 5.65\mathrm{E12} * B_{\mathrm{ext}} \quad (3)$$

We tested how sensitive changing the slopes and intercepts were because the initial best fit resulted in negative values in the 1970s, which is not plausible. To circumvent this issue, we increased the intercepts with steps of 0.5E11 until it started to negatively impact the correlations ($r^2 = 0.61$ and $r^2 = 0.40$ for the western and eastern boxes, respectively) and mean squared errors and used the corresponding slopes and intercepts as used in equations (2) and (3) in our calculations back in time.

The western box (Figures 6d and 6e) shows equal or higher agreement compared to the total region for both GFED TPM and MOPITT CO, explaining 47% and 32%, respectively (Table 1). The IAV for the western box is similar to the IAV of the total region. This is not the case for the eastern box (Figures 7d and 7e). Although the monthly aggregated visibility observations do show a linear relationship ($r^2 = 0.40$) on a monthly time step (Figures 7a–7c), there are no significant relationships with GFED TPM emissions or MOPITT CO

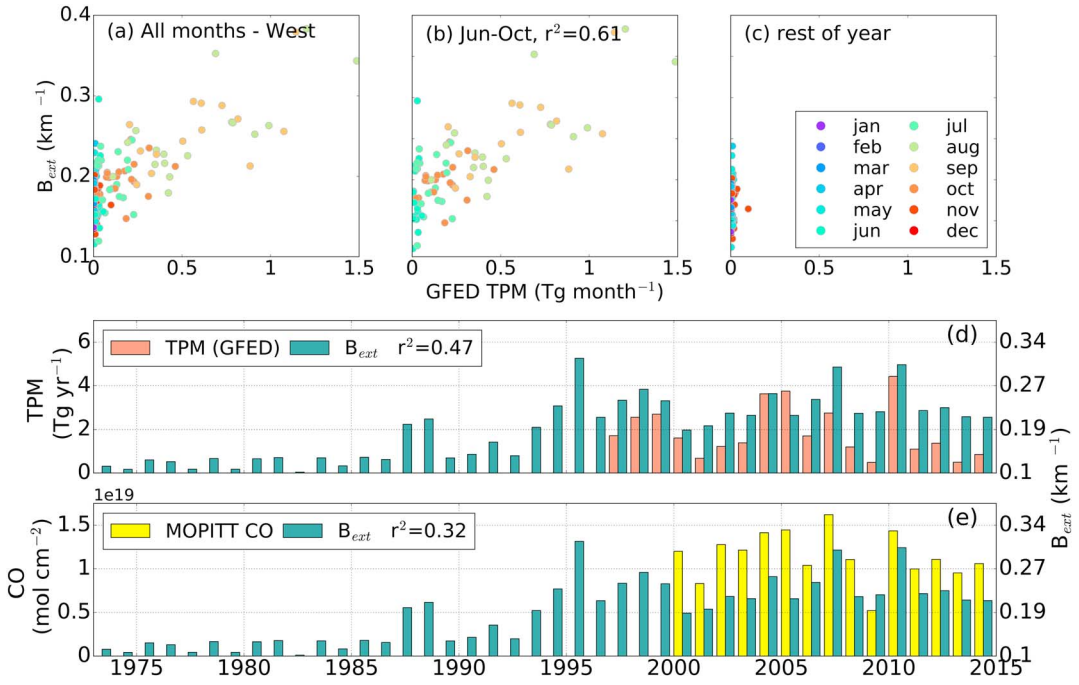

Figure 6. Relations between monthly B_{ext} observations and GFED TPM emissions for the overlapping time period 1997–2014, and annual B_{ext}, TPM and CO time series in the western box (red square in Figure 2). Figure 6a shows all months, Figure 6b the data points for the months of the fire season from June to October, and Figure 6c the remaining months. Dark green indicates the visibility-based annual B_{ext} emissions (1974–2014), which are compared with (d) GFED-based TPM emissions (1997–2014) and (e) MOPITT CO concentrations (2000–2014) for the same region.

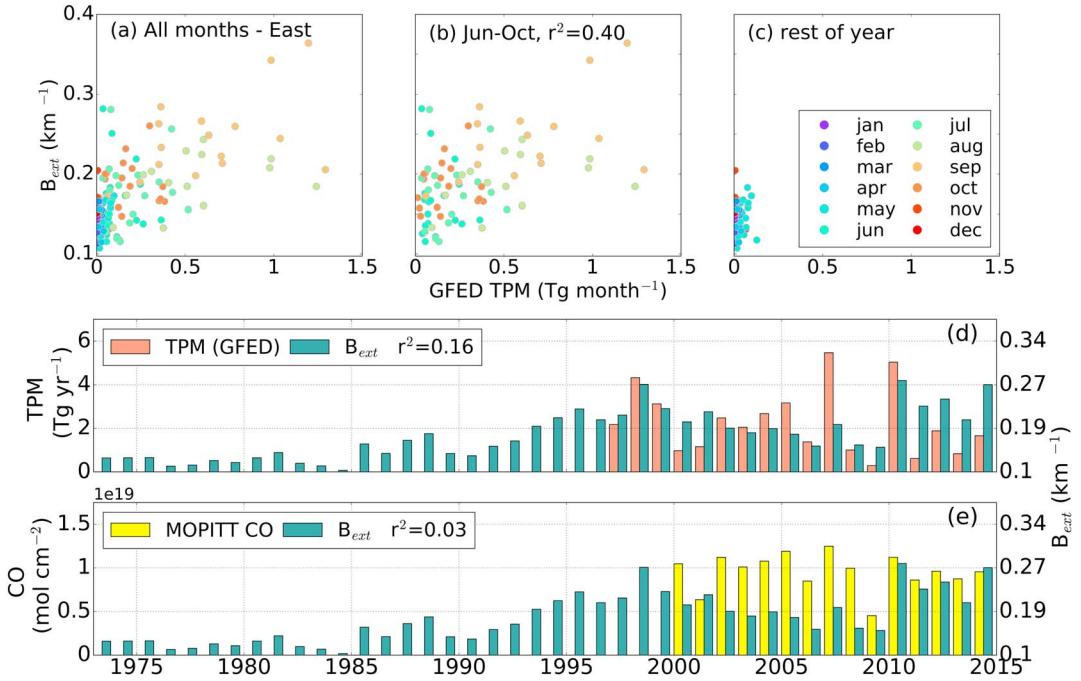

Figure 7. Relations between monthly B_{ext} observations and GFED TPM emissions for the overlapping time period 1997–2014, and annual B_{ext}, TPM and CO time series in the eastern box (black square in Figure 2). Figure 7a shows all months, Figure 7b the data points for the months of the fire season from June to October, and Figure 7c the remaining months. Dark green indicates the visibility-based TPM emissions (1974–2014), which are compared with (d) annual GFED TPM emissions (1997–2014) and (e) MOPITT CO concentrations (2000–2014) for the same region.

concentrations with B_{ext} (Table 1). The biggest discrepancies between visibility-based B_{ext} and GFED TPM emissions are found in 2007, where GFED shows higher values and the years 2001, 2002, and from 2011 onward, where visibility-based TPM is higher. In the discussion we touch upon potential reasons behind these differences between the boxes.

4.3. Deforestation as Driver of IAV in Fire Activity

We finally compared visibility-based B_{ext} with forest loss data sets to understand to what degree the fire signal may be explained by deforestation. For this comparison we mainly focused on the whole study region.

Figure 8a shows that annual VOD-based net forest loss in the study region explained 31% of the variability in the B_{ext} signal (Table 2). The high-fire years in 1995 and 2010 are captured in both data sets, whereas VOD shows higher deforestation rates from 2003 to 2006. Figure 8b shows that PRODES-based deforestation for the provinces of Acre, Mato Grosso, Pará, Rondônia, and Tocantins cannot explain the B_{ext} signal. The IAV between both data sets partly agrees, especially during the 1990s, including the peak in 1995. The poor correlation is for a large part due to disagreement between PRODES and the visibility-based results on emissions from 2009 onward, including the peak in high-fire year 2010.

We compared the annual averaged B_{ext} with the FAO-based carbon emissions related to deforestation from an updated version of *Houghton* [2003]. Correlations with B_{ext} were poor (Figure 8c and Table 2). One of the most striking discrepancies is that the FAO-based carbon emissions related to forest fires from the 1970s to the early 1990s were higher than the visibility-based emissions. In addition, there are key differences in IAV (as was the case when comparing against the two deforestation data sets). For example, 1996 and 2000, years with little visibility-based emissions, show higher values for the FAO-based results. On the other hand, 2010 was a high-fire year, according to the visibility-based data set, which did not show up in the FAO-based data set.

Although the eastern region did not show any significant relations for the B_{ext} signal with GFED TPM and MOPITT CO, VOD-based net forest loss explained 33%, whereas FAO-based carbon emissions did explain

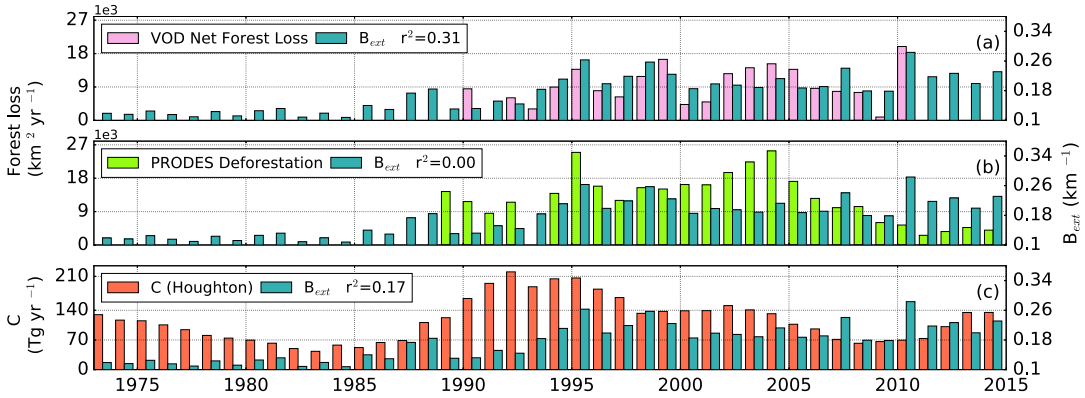

Figure 8. Annual estimates of fire emissions and forest loss for the whole study region (Figure 2). In all plots dark green indicates the annual averaged visibility-based B_{ext} (1974–2014), which are compared with (a) VOD-based net forest loss (1990–2010), (b) summed PRODES deforestation for the provinces of Acre, Mato Grosso, Rondônia, Pará, and Tocantins (1989–2014, and (c) averaged FAO emissions attributed to deforestation fires for Brazil and Bolivia.

18% of the B_{ext} IAV for the eastern region. For the western region both VOD and Houghton explained, respectively, 23% and 9% of the B_{ext} signal (Table 2).

We converted the visibility-based B_{ext} signal to TPM emissions based on the linear relationships with GFED TPM mentioned before for the different regions and to carbon emissions using emission factors from GFED. We then compared the visibility-based carbon emissions with the summed FAO-based carbon emissions related to deforestation based on *Houghton* [2003] for Brazil and Bolivia at a decadal scale. The footprint of the two data sets differs because the FAO-based values are from all of Brazil and Bolivia, but our study region (Figure 2) covered the region with the highest fire emissions from 1997 to 2014 (Figure 2). Our estimates are therefore conservative. From the 1970s to the 1980s, the FAO-based data set and the visibility-based emissions show opposing trends, with a large increase (+747%) for the visibility-based carbon emissions and a decrease (−32%) for FAO-based deforestation-linked fire emissions (Figure 9). The large relative increase in the visibility data set is mostly because of low fire emissions in the 1970s. For both data sets the 1990s had the highest fire emissions. Both data sets also show a decrease from the 1990s to the 2000s, although the FAO-based emissions decreased more strongly (−41%) than the visibility-based emissions (−8%).

5. Discussion

5.1. Visibility as Fire Indicator

On a local level, the good agreement ($r^2 = 0.84$ with monthly time step and $r^2 = 0.79$ with annual data) between visibility-based TPM and in situ observed PM_{10} at Alta Floresta station (Figure 5) indicated that visibility is strongly linked to aerosol loads and can be used, with limitations, as a proxy for fire emissions. This has been shown earlier to be the case as well in Indonesia [*Field et al.*, 2009]. This also holds on larger scales; for the western box the pattern of the visibility-based signal agreed reasonable with the GFED-derived TPM emissions ($r^2 = 0.61$) and MOPITT CO concentrations ($r^2 = 0.42$) for the overlapping time period. For the whole

Table 2. Correlations Between Annual Averaged B_{ext} for June–October and Annual VOD Net Forest Loss (1990–2010), Annual PRODES Deforestation Summed for the Provinces Acre, Mato Grosso, Rondônia, Pará, and Tocantins (1989–2014) and Carbon Emissions From an Updated Version of *Houghton* [2003] for Brazil (Eastern Box Only) and the Average of Boliva and Brazil (Western Box and Whole Region) (1973–2014)

	Visibility TPM r^2		
	West [7°S–17°S, 58°W–68°W]	East [7°S–17°S, 48°W–58°W]	Total Region [7°S–17°S, 48°W–68°W]
VOD	0.23* (*p*)	0.33* (*p*)	0.31* (*p*)
PRODES	0.02* (*p*)	0.04 (*p*)	0.00
Houghton	0.09* (*s*)	0.18* (*s*)	0.17* (*s*)

*Pearson (*p*) or Spearman (*s*) correlation significant at $p < 0.01$.

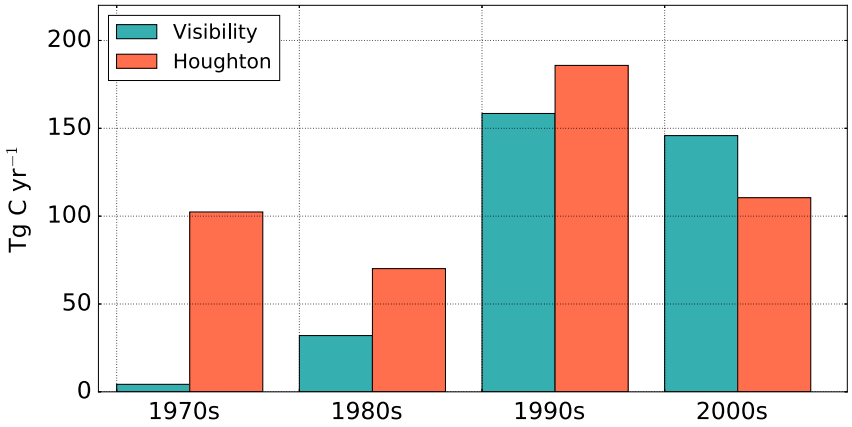

Figure 9. Visibility-based carbon emissions for the whole study region and carbon emissions related to deforestation fires for Brazil and Bolivia based on FAO-deforestation data and an updated version of *Houghton* [2003] for 10 year periods. The 1970s decade covers the time period from 1973 to 1980.

region (the western and eastern boxes combined) results were less good; IAV of B_{ext} explained 47% of GFED TPM emissions and only 18% of MOPITT CO concentrations. The unexplained variability is likely due to measurement errors in the visibility signal and issues related to its spatial inhomogeneous network, the conversion to B_{ext}, other sources that impact B_{ext}, and the effects of atmospheric transport and chemistry. The error in atmospheric transport may be larger for the eastern box because variability in wind patterns is larger than in the western box, and smoke gets more concentrated in the western box because of the proximity to the Andes (Figure 1). Given the overall reasonable results, our findings may be suitable to fulfill the need for more detailed information on land use and land cover change over the tropics before the satellite era [*Willcock et al*., 2016].

Annual averaged B_{ext} values, and thus fire emissions, were relatively low over the first part of the time series from 1973 until the first high-fire years in 1987 and 1988. These two relatively high-fire years were followed by some low-fire years, after which fire emissions started to increase over the 1990s, with 1995 being the peak year over the 1990s, which was also a high-fire year according to fire season severity predictions based on sea surface temperature anomalies [*Chen et al*., 2011]. After 1995 fire emissions were higher than the pre-1987 values. During the 2000s there was a general decrease, although 2010 was the highest fire year in our data set. This downward trend is also reported by the Global Forest Change project and satellite-observed burned area, suggesting that fires and deforestation are linked over that time period [*Hansen et al*., 2013; *Fanin and van der Werf*, 2015].

The first high-fire years 1987 and 1988 correspond to two El Niño years, which are associated with dryer conditions over the burning regions [*Chen et al*., 2011], although earlier in the 1970s no increase in fire emissions was observed during El Niño years. This suggests that fire in the region increased due to conversion of forest to other land uses, similar to what was observed in Indonesia [*Field et al*., 2009]. A key difference with Indonesia is the stronger control of El Niño–Southern Oscillation (ENSO) over drought and thus fire emissions. At a decadal scale the trend of increasing fires from 1970 to the 1990s corresponds with the results based on country statistics of *Mouillot and Field* [2005] for South America. However, the timing of the increase is different. *Mouillot and Field* [2005] suggested that the strongest increase was during the 1980s, while our data indicated that this was a decade later in the 1990s. There is thus apparently a difference between what was reported by countries and what is actually seen in the data, assuming that the average distance of deforestation to the stations before the 1990s showed equally little variability as after the 1990s. Another reason could be that fire was used to a smaller extent in the early part of our analysis to convert forest to other land uses.

The correlations between B_{ext} and other data sets we found for the whole region were negatively impacted by the eastern box, which showed for both the GFED TPM and MOPITT CO comparisons lower agreement than the western box (Table 1). The most likely reason for this is the geographical location of the western box adjacent to the Andes. The prevailing wind during the dry season is from the northeast [*Killeen et al*., 2007], and thus, the smoke will be concentrated in front of the Andes mountain range (Figure 1). This implies

that the visibility signal of the western box is probably representative for a much larger region. We tested this hypothesis by comparing the visibility signal for the western box only with the GFED TPM emissions for the whole region (i.e., the summed values for the two 10° × 10° from Figure 2, 7°S–17°S, 48°W–68°W). We found that 65% of the GFED TPM time series could be explained by B_{ext}, which is 18% more than the comparison of the visibility signal for the western region, with the GFED TPM emissions for the western region ($r^2 = 0.47$, Table 1). Comparing MOPITT CO concentrations and VOD net forest loss over the whole region with the B_{ext} for the western box only also revealed that B_{ext} could explain more of the interannual variability with an increase of 8% and 7% for correlations between B_{ext} with MOPITT CO concentrations and B_{ext} with VOD-based net forest loss, respectively. This also explains why the combined visibility observations of the eastern and western boxes still explained 47% of GFED TPM emissions and 18% of MOPITT CO concentrations (Table 1 and Figure 4). Future research could investigate this in more detail including regional transport and atmospheric chemistry modeling.

For the western box, the overlapping time period of visibility with GFED (1997–2014) showed for most years an agreement in IAV, including the high-fire years in 1999, 2004, and 2010. However, in 2001, 2005, and 2006 the GFED and visibility-based fire signal disagreed, potentially due to uncertainties in both data sets or changes in atmospheric transport. A potential error in GFED is related to assigning the burned area to the wrong fuel classes. For example, if most of the burned area occurs in open landscapes but is assigned to deforestation fires, then emissions are overestimated. Visibility observations are also prone to errors, due to the nature of this human-observed proxy and our approach of combining the different records. Furthermore, the WMO stations are not evenly distributed over the region, which could have the effect that fires that occurred close to a station will have a relatively large effect on the average signal and that some fires may be missed, because there is no station located near or downwind from those fires.

5.2. Deforestation as Driver of Fire Activity

To answer the question to what extent deforestation can explain trends and IAV in fire emissions, we compared B_{ext} with several deforestation data sets. For the whole study region VOD-based forest loss explained 31% of the fire signal, which suggests that deforestation and fires were coupled to some degree in this region for the overlapping time period from 1990 to 2014. PRODES deforestation explained little of the fire signal. We used the summed values of Acre, Mato Grosso, Rondônia, Pará, and Tocantins for PRODES. These are the provinces within the Legal Amazon closest to the two boxes, and results did not improve when we used PRODES data for the whole Legal Amazon or decreased our subset to a smaller number of provinces. One potential reason is that PRODES does not capture forest degradation, which caused high fire emissions in, for example, the 2010 dry year [*Fanin and van der Werf*, 2015]. Furthermore, we assumed that the state statistics for the five Brazilian provinces used were representative for the western box, because we expected the source regions to be largely from these provinces as a result of the prevailing wind direction. To some degree the comparison is not fair because PRODES is limited to Brazil, while the visibility signal potentially will also be affected by dynamics in Bolivia and Peru. Future research could include specific source regions, thus providing more insight into the actual area that is represented by the visibility signal.

Although correlations were higher, the comparisons with VOD-based net forest loss also suffered from limitations in the data sets. This forest loss data set captures mainly large-scale forest losses and in areas with many small-scale degradation events, VOD-based forest loss tends to overestimate, which could explain why the VOD-based interannual variability provides overall much higher values in 2003 to 2006 compared to the visibility-based fire emissions. Also, regrowth within a pixel is observed which can offset some of the signal [*van Marle et al*., 2016].

Overall, the comparison with the VOD-based deforestation data set provided evidence that deforestation is what at least partly drives these fires ($r^2 = 0.23$ and $r^2 = 0.33$ for the western box and eastern box, respectively, and $r^2 = 0.31$ for the whole region), although fires are a complex mix of deforestation, degradation, and natural causes. After deforestation, the land cover or use may change leading initially to an increase in burned area to maintain an open landscape or remove leftover debris. This is not captured in the deforestation data but will impact the visibility signal although fuel loads are, in general, lower in these types of fires [*van Leeuwen et al*., 2014]. Overall, it is difficult to explain the fire pattern without taking deforestation into account supporting *Reddington et al*. [2015], who concluded that deforestation fires dominate regional air quality

impacts in Brazil. Our results are also in line with the findings of *Morton et al*. [2008], who showed that most fires in the Amazon during the 2000s were related to conversion of forest to agricultural land. We therefore cautiously conclude that the forest to other land use conversion started slowly at the end of the 1980s and increased strongly during the 1990s with accompanying deforestation fires. We are cautious, because the drivers of deforestation could have changed over time, influenced by changes in infrastructure, logging, and governmental subsidies [*Moran*, 1993; *Fearnside*, 2005; *Rudel*, 2007; *Cochrane*, 2009], and not all deforestation includes fire. An analysis of the GFED time series showed that the ratio between deforestation and nondeforestation fire emissions is relatively stable though, with on average 55% of fire emissions stemming from deforestation fires (1997–2015).

Finally, the FAO-based deforestation emissions could explain 9% of the fire signal in the western box and 18% of the fire signal in the eastern box over 1973–2014. There was less agreement between B_{ext} and FAO than between B_{ext} and VOD, and this is probably the result of what VOD and FAO observe and how IAV is captured. VOD observes the net change in biomass, whereas FAO FRA only observes the conversion from forest to another land use type. For example, changes in biomass due to understory fires or from fires that do not lead to land use change may be detected by VOD, but not by PRODES and FAO; a potential explanation of why the peak in 2010 is missed. Furthermore, the IAV of carbon emissions in the bookkeeping method of *Houghton* [2003] is based on 5 year estimates of FAO FRA in combination with annual changes in cropland and pastures, thus not fully capturing IAV. The third reason for differences is the scale on which deforestation is observed. For most comparisons we found a better agreement with visibility and other data sets for the western box, compared to the eastern box. However, the FAO-based values compared better for the eastern box. Since the deforestation estimates are on a country level and not separated by province, this could be the result of discontinuity between Brazilian and Bolivian data. Although the two boxes we selected include the region with most fires over 1997–2014, this does not mean that all IAV for Brazil and Bolivia is captured.

This potential mismatch in footprint obviously also impacted the results on a decadal scale. The biggest difference between the FAO-based and our visibility-based fire emission estimates was in the early part of our time series from the 1970s until the first half of the 1990s. The visibility data indicated a gradual increase from very low to moderate emissions, while FAO-based emissions changed from relatively high to moderate. FAO data are based on the country totals of Brazil and Bolivia and therefore also captured carbon emissions related to deforestation occurring outside the Amazon region. Both data sets do agree on decadal averages for the 1990s and 2000s.

6. Conclusions

We have reconstructed fire emissions with an annual time step from 1973 to 2014 based on visibility observations from weather stations across the Amazon. Our study region encompassed the Arc of Deforestation and Bolivia, and we compared and constrained our results with satellite-derived fire emission estimates for the overlapping 1997–2014 period and MOPITT CO concentrations over the 2000–2014 period. These comparisons indicated that, with limitations, visibility can be a useful proxy for fire emissions in the Amazon. In general, the signal improves towards the western part of the Amazon where smoke gets more concentrated, because the Andes blocks the overall eastern winds.

The visibility signal showed that there was relatively little fire activity until 1987, after which fires increased and plateaued in the 1990s and 2000s before leveling off more recently. Substantial interannual variability has been present since the late 1980s and was partly related to ENSO, and comparisons with deforestation data sets showed that fires and deforestation were linked here although not all deforestation data sets were suitable for direct comparison with the visibility signal. Our estimates point towards lower (fire-driven) deforestation in the 1970s than found in FAO-based data sets. In our work we have assumed that the variability in B_{ext} was directly proportional to emissions, omitting changes due to variability in atmospheric transport as well as changes due to spatial variability in the location of fire and deforestation events. Initial estimates indicated that variability in wind patterns was small as was the average distance of fire to the stations. While the errors due to this seem relatively small, a more extensive and spatially explicit study including a regional transport model is needed to better understand what impact progressing fire and deforestation fronts had on the observations.

Acknowledgments

We would like to thank Enrico Dammers, Benjamin Aouizerats, and Douglas Morton for useful discussions. Furthermore, we acknowledge INPE for making the PRODES publicly available (http://www.obt.inpe.br/prodes/index.php). GFED4s data is publicly available at http://www.globalfiredata.org/data.html. Visibility observations were obtained from the NOAA National Climatic Data Center Integrated Surface Database (https://catalog.data.gov/dataset/integrated-surface-global-hourly-data). FAO-based carbon emissions related to deforestation, the VOD-based net forest loss, and the visibility-based time series developed during this research can be requested via the corresponding author. This research was funded by the European Research Council (ERC) grant 280061 (M.v.M. G.v.d.W.), NASA Atmospheric Chemistry Modeling and Analysis Program (R.F.), NASA Carbon Monitoring System (R.H.), FAPESP grant 2003/05014-0 (P.A.), and CNPq (P.A.). We thank two reviewers for their constructive comments and helpful suggestions on an earlier version of this manuscript.

References

Akagi, S. K., R. J. Yokelson, C. Wiedinmyer, M. J. Alvarado, J. S. Reid, T. Karl, J. D. Crounse, and P. O. Wennberg (2011), Emission factors for open and domestic biomass burning for use in atmospheric models, *Atmos. Chem. Phys.*, *11*(9), 4039–4072, doi:10.5194/acp-11-4039-2011.

Aragão, L. E. O. C., B. Poulter, J. B. Barlow, L. O. Anderson, Y. Malhi, S. Saatchi, O. L. Phillips, and E. Gloor (2014), Environmental change and the carbon balance of Amazonian forests, *Biol. Rev.*, *89*(4), 913–931, doi:10.1111/brv.12088.

Artaxo, P., F. Gerab, M. A. Yamasoe, and J. V. Martins (1994), Fine mode aerosol composition at three long-term atmospheric monitoring sites in the Amazon Basin, *J. Geophys. Res.*, *99*(D11), 22,857–22,868, doi:10.1029/94JD01023.

Bevan, S. L., P. R. J. North, W. M. F. Grey, S. O. Los, and S. E. Plummer (2009), Impact of atmospheric aerosol from biomass burning on Amazon dry-season drought, *J. Geophys. Res.*, *114*, D09204, doi:10.1029/2008JD011112.

Chang, D., Y. Song, and B. Liu (2009), Visibility trends in six megacities in China 1973–2007, *Atmos. Res.*, *94*(2), 161–167, doi:10.1016/j.atmosres.2009.05.006.

Che, H., X. Zhang, Y. Li, Z. Zhou, and J. J. Qu (2007), Horizontal visibility trends in China 1981–2005, *Geophys. Res. Lett.*, *34*, L24706, doi:10.1029/2007GL031450.

Chen, Y., J. T. Randerson, D. C. Morton, R. S. DeFries, G. J. Collatz, P. S. Kasibhatla, L. Giglio, Y. Jin, and M. E. Marlier (2011), Forecasting fire season severity in South America using sea surface temperature anomalies, *Science*, *334*(6057), 787–791, doi:10.1126/science.1209472.

Chen, Y., D. C. Morton, Y. Jin, G. J. Collatz, P. S. Kasibhatla, G. R. van der Werf, R. S. DeFries, and J. T. Randerson (2013), Long-term trends and interannual variability of forest, savanna and agricultural fires in South America, *Carbon Manage.*, *4*(6), 617–638, doi:10.4155/cmt.13.61.

Cochrane, M. A. (2003), Fire science for rainforests, *Nature*, *421*(6926), 913–919, doi:10.1038/nature01437.

Cochrane, M. A. (2009), Fire, land use, land cover dynamics, and climate change in the Brazilian Amazon, in *Tropical Fire Ecology: Climate Change Land Use, and Ecosystem Dynamics*, pp. 389–426, Springer, Chichester, U. K., doi:10.1007/978-3-540-77381-8_14.

Davidson, E. A., et al. (2012), The Amazon basin in transition, *Nature*, *481*(7381), 321–328, doi:10.1038/nature10717.

Doyle, M., and S. Dorling (2002), Visibility trends in the UK 1950–1997, *Atmos. Environ.*, *36*(19), 3161–3172, doi:10.1016/S1352-2310(02)00248-0.

Edwards, D. P., G. Pétron, P. C. Novelli, L. K. Emmons, J. C. Gille, and J. R. Drummond (2006), Southern Hemisphere carbon monoxide interannual variability observed by Terra/Measurement of Pollution in the Troposphere (MOPITT), *J. Geophys. Res.*, *111*, D16303, doi:10.1029/2006JD007079.

Fanin, T., and G. R. van der Werf (2015), Relationships between burned area, forest cover loss, and land cover change in the Brazilian Amazon based on satellite data, *Biogeosciences*, *12*(20), 6033–6043, doi:10.5194/bg-12-6033-2015.

Fearnside, P. M. (2005), Deforestation in Brazilian Amazonia: History, rates, and consequences, *Conserv. Biol.*, *19*(3), 680–688, doi:10.1111/j.1523-1739.2005.00697.x.

Field, R. D., G. R. van der Werf, and S. S. P. Shen (2009), Human amplification of drought-induced biomass burning in Indonesia since 1960, *Nat. Geosci.*, *2*(3), 185–188, doi:10.1038/ngeo443.

Field, R. D., et al. (2016), Indonesian fire activity and smoke pollution in 2015 show persistent nonlinear sensitivity to El Niño-induced drought, *Proc. Natl. Acad. Sci. U.S.A.*, *113*, 9204–9209, doi:10.1073/pnas.1524888113.

Food and Agriculture Organization of the United Nations (2012), *Global Forest Land-Use Change 1990–2005*, Food and Agriculture Organization of the United Nations and Joint Research Centre, Rome.

Giglio, L., J. T. Randerson, and G. R. van der Werf (2013), Analysis of daily, monthly, and annual burned area using the fourth-generation global fire emissions database (GFED4), *J. Geophys. Res. Biogeosci.*, *118*, 317–328, doi:10.1002/jgrg.20042.

Gonçalves, W. A., L. A. T. Machado, and P.-E. Kirstetter (2015), Influence of biomass aerosol on precipitation over the Central Amazon: An observational study, *Atmos. Chem. Phys.*, *15*(12), 6789–6800, doi:10.5194/acp-15-6789-2015.

Hansen, M. C., et al. (2013), High-resolution global maps of 21st-century forest cover change, *Science*, *342*(6160), 850–853, doi:10.1126/science.1244693.

Heil, A., and J. G. Goldammer (2001), Smoke-haze pollution: A review of the 1997 episode in Southeast Asia, *Reg. Environ. Change*, *2*(1), 24–37, doi:10.1007/s101130100021.

Houghton, R. A. (2003), Revised estimates of the annual net flux of carbon to the atmosphere from changes in land use and land management 1850–2000, *Tellus, Ser. B*, *55*(2), 378–390, doi:10.1034/j.1600-0889.2003.01450.x.

Houghton, R. A., D. L. Skole, and D. S. Lefkowitz (1991), Changes in the landscape of Latin America between 1850 and 1985 II. Net release of CO_2 to the atmosphere, *For. Ecol. Manage.*, *38*(3–4), 173–199, doi:10.1016/0378-1127(91)90141-H.

Husar, R. B., J. D. Husar, and L. Martin (2000), Distribution of continental surface aerosol extinction based on visual range data, *Atmos. Environ.*, *34*(29–30), 5067–5078, doi:10.1016/S1352-2310(00)00324-1.

Johnston, F. H., S. B. Henderson, Y. Chen, J. T. Randerson, M. Marlier, R. S. DeFries, P. Kinney, D. M. J. S. Bowman, and M. Brauer (2012), Estimated global mortality attributable to smoke from landscape fires, *Environ. Health Perspect.*, *120*(5), 695–701, doi:10.1289/ehp.1104422.

Kaiser, J. W., et al. (2012), Biomass burning emissions estimated with a global fire assimilation system based on observed fire radiative power, *Biogeosciences*, *9*(1), 527–554, doi:10.5194/bg-9-527-2012.

Kalnay, E., et al. (1996), The NCEP/NCAR 40-year reanalysis project, *Bull. Am. Meteorol. Soc.*, *77*(3), 437–471, doi:10.1175/1520-0477(1996)077<0437:TNYRP>2.0.CO;2.

Killeen, T. J., M. Douglas, T. Consiglio, P. M. Jørgensen, and J. Mejia (2007), Dry spots and wet spots in the Andean hotspot, *J. Biogeogr.*, *34*(8), 1357–1373, doi:10.1111/j.1365-2699.2006.01682.x.

Li, C., R. V. Martin, B. L. Boys, A. van Donkelaar, and S. Ruzzante (2016), Evaluation and application of multi-decadal visibility data for trend analysis of atmospheric haze, *Atmos. Chem. Phys.*, *16*(4), 2435–2457, doi:10.5194/acp-16-2435-2016.

Liu, C., et al. (2011), Application of SCIAMACHY and MOPITT CO total column measurements to evaluate model results over biomass burning regions and Eastern China, *Atmos. Chem. Phys.*, *11*(12), 6083–6114, doi:10.5194/acp-11-6083-2011.

Liu, Y. Y., A. I. J. M. van Dijk, R. A. M. de Jeu, J. G. Canadell, M. F. McCabe, J. P. Evans, and G. Wang (2015), Recent reversal in loss of global terrestrial biomass, *Nat. Clim. Change*, *5*(5), 470–474, doi:10.1038/nclimate2581.

Livesey, N. J., J. A. Logan, M. L. Santee, J. W. Waters, R. M. Doherty, W. G. Read, L. Froidevaux, and J. H. Jiang (2013), Interrelated variations of O_3, CO and deep convection in the tropical/subtropical upper troposphere observed by the Aura Microwave Limb Sounder (MLS) during 2004–2011, *Atmos. Chem. Phys.*, *13*(2), 579–598, doi:10.5194/acp-13-579-2013.

Logan, J. A., I. Megretskaia, R. Nassar, L. T. Murray, L. Zhang, K. W. Bowman, H. M. Worden, and M. Luo (2008), Effects of the 2006 El Niño on tropospheric composition as revealed by data from the Tropospheric Emission Spectrometer (TES), *Geophys. Res. Lett.*, *35*, L03816, doi:10.1029/2007GL031698.

MacDicken, K. G. (2015), Global forest resources assessment 2015: What, why and how?, *For. Ecol. Manage.*, *352*, 3–8, doi:10.1016/j.foreco.2015.02.006.

Maenhaut, W., M.-T. Fernández-Jiménez, I. Rajta, and P. Artaxo (2002), Two-year study of atmospheric aerosols in Alta Floresta, Brazil: Multielemental composition and source apportionment, *Nucl. Instrum. Methods Phys. Res., Sect. B*, *189*(1–4), 243–248, doi:10.1016/S0168-583X(01)01050-3.

Mahowald, N. M., J. A. Ballantine, J. Feddema, and N. Ramankutty (2007), Global trends in visibility: Implications for dust sources, *Atmos. Chem. Phys.*, *7*, 3309–3339, doi:10.5194/acp-7-3309-2007.

Marlier, M. E., R. S. DeFries, A. Voulgarakis, P. L. Kinney, J. T. Randerson, D. T. Shindell, Y. Chen, and G. Faluvegi (2012), El Niño and health risks from landscape fire emissions in Southeast Asia, *Nat. Clim. Change*, *3*(2), 131–136, doi:10.1038/nclimate1658.

Marlon, J. R., P. J. Bartlein, A. L. Daniau, S. P. Harrison, S. Y. Maezumi, M. J. Power, W. Tinner, and B. Vanniére (2013), Global biomass burning: A synthesis and review of Holocene paleofire records and their controls, *Quat. Sci. Rev.*, *65*, 5–25, doi:10.1016/j.quascirev.2012.11.029.

Martin, S. T., et al. (2010), Sources and properties of Amazonian aerosol particles, *Rev. Geophys.*, *48*, RG2002, doi:10.1029/2008RG000280.

Mieville, A., C. Granier, C. Liousse, B. Guillaume, F. Mouillot, J.-F. Lamarque, J.-M. Grégoire, and G. Pétron (2010), Emissions of gases and particles from biomass burning during the 20th century using satellite data and an historical reconstruction, *Atmos. Environ.*, *44*(11), 1469–1477, doi:10.1016/j.atmosenv.2010.01.011.

Moran, E. F. (1993), Deforestation and land use in the Brazilian Amazon, *Hum. Ecol.*, *21*(1), 1–21, doi:10.1007/BF00890069.

Morton, D. C., R. S. DeFries, Y. E. Shimabukuro, L. O. Anderson, E. Arai, F. del Bon Espirito-Santo, R. Freitas, and J. Morisette (2006), Cropland expansion changes deforestation dynamics in the southern Brazilian Amazon, *Proc. Natl. Acad. Sci. U.S.A.*, *103*(39), 14,637–14,641, doi:10.1073/pnas.0606377103.

Morton, D. C., R. S. DeFries, J. T. Randerson, L. Giglio, W. Schroeder, and G. R. van der Werf (2008), Agricultural intensification increases deforestation fire activity in Amazonia, *Global Change Biol.*, *14*(10), 2262–2275, doi:10.1111/j.1365-2486.2008.01652.x.

Mouillot, F., and C. B. Field (2005), Fire history and the global carbon budget: A 1° × 1° fire history reconstruction for the 20th century, *Global Change Biol.*, *11*(3), 398–420, doi:10.1111/j.1365-2486.2005.00920.x.

Nepstad, D. C., et al. (1999), No Title, *Nature*, *398*(6727), 505–508, doi:10.1038/19066.

Nepstad, D., et al. (2009), The end of deforestation in the Brazilian Amazon, *Science*, *326*(5958), 1350–1351, doi:10.1126/science.1182108.

Power, M. J., J. R. Marlon, P. J. Bartlein, and S. P. Harrison (2010), Fire history and the Global Charcoal Database: A new tool for hypothesis testing and data exploration, *Palaeogeogr. Palaeoclimatol. Palaeoecol.*, *291*(1–2), 52–59, doi:10.1016/j.palaeo.2009.09.014.

Randerson, J. T., Y. Chen, G. R. van der Werf, B. M. Rogers, and D. C. Morton (2012), Global burned area and biomass burning emissions from small fires, *J. Geophys. Res.*, *117*, G04012, doi:10.1029/2012JG002128.

Reddington, C. L., E. W. Butt, D. A. Ridley, P. Artaxo, W. T. Morgan, H. Coe, and D. V. Spracklen (2015), Air quality and human health improvements from reductions in deforestation-related fire in Brazil, *Nat. Geosci.*, *8*(10), 768–771, doi:10.1038/ngeo2535.

Rudel, T. K. (2007), Changing agents of deforestation: From state-initiated to enterprise driven processes, 1970–2000, *Land Policy*, *24*(1), 35–41, doi:10.1016/j.landusepol.2005.11.004.

Schichtel, B. A., R. B. Husar, S. R. Falke, and W. E. Wilson (2001), Haze trends over the United States, 1980–1995, *Atmos. Environ.*, *35*(30), 5205–5210, doi:10.1016/S1352-2310(01)00317-X.

Shimabukuro, Y. E., G. T. Batista, E. M. K. Mello, J. C. Moreira, and V. Duarte (1998), Using shade fraction image segmentation to evaluate deforestation in Landsat Thematic Mapper images of the Amazon Region, *Int. J. Remote Sens.*, *19*(3), 535–541, doi:10.1080/014311698216152.

van der Werf, G. R., J. T. Randerson, L. Giglio, G. J. Collatz, M. Mu, P. S. Kasibhatla, D. C. Morton, R. S. DeFries, Y. Jin, and T. T. van Leeuwen (2010), Global fire emissions and the contribution of deforestation, savanna, forest, agricultural, and peat fires (1997–2009), *Atmos. Chem. Phys.*, *10*(23), 11,707–11,735, doi:10.5194/acp-10-11707-2010.

van Leeuwen, T. T., et al. (2014), Biomass burning fuel consumption rates: A field measurement database, *Biogeosciences*, *11*(24), 7305–7329, doi:10.5194/bg-11-7305-2014.

van Marle, M. J. E., G. R. van der Werf, R. A. M. de Jeu, and Y. Y. Liu (2016), Annual South American forest loss estimates based on passive microwave remote sensing (1990–2010), *Biogeosciences*, *13*(2), 609–624, doi:10.5194/bg-13-609-2016.

Willcock, S., et al. (2016), Land cover change and carbon emissions over 100 years in an African biodiversity hotspot, *Global Change Biol.*, *22*(8), 2787–2800, doi:10.1111/gcb.13218.

World Meteorological Organization (1996), *Guide to Meteorological Instruments and Methods of Observation*, 6th ed., Secretariat of the World Meteorological Organization, Geneva, Switzerland.